Amin et al | Article 10934
J Pure Appl Microbiol. 2026;20(1):622-641. doi: 10.22207/JPAM.20.1.48
Received: 03 September 2025 | Accepted: 15 January 2026
Published Online: 02 March 2026

P-ISSN: 0973-7510; E-ISSN: 2581-690X

RESEARCH ARTICLE OPEN ACCESS

Curcuma longa-mediated Biogenic and Eco-friendly Silver Nanoparticles with Promising Antibacterial Activity

Durdana Sadaf Amin[1], A. Najitha Banu[1] and Jibanananda Mishra[2,3]*

[1]School of Bioengineering and Biosciences, Lovely Professional University, Phagwara, Punjab, India.
[2]School of Biosciences, RIMT University, Mandi Gobindgarh, Punjab, India.
[3]AAL Biosciences Research Pvt. Ltd., 287, Barwala Industrial Estate, Alipur, Bhanoo, Haryana, India.

Abstract

An affordable and environmentally suitable method for generating AgNPs (silver nanoparticles) was attained utilizing an aqueous rhizome extract of *Curcuma longa* (*Cl*). A detailed analysis of the synthesized *Cl*-AgNPs was performed utilizing a number of analytical techniques, comprising UV-vis spectroscopy, DLS, FTIR, XRD, SEM, EDAX along with elemental mapping, and TEM. UV-vis spectroscopy substantiated successful synthesis of *Cl*-AgNPs, as there was a change in the surface plasmon resonance (SPR) peak from λ_{max} 416 nm to λ_{max} 423 nm. XRD showed that the nature of *Cl*-AgNPs is crystalline and possess a face-centered cubic (FCC) structure. The average size of the crystallites was observed to be 16 nm through Debye-Scherrer equation. Further, SEM/TEM analysis depicted that the size range of the NPs are of 30-70 nm and spherical in shape. Additionally, antibacterial effect of the *Cl*-AgNPs were assessed through the broth dilution method and well-diffusion method to find out the MIC and MBC. Results showed *Cl*-AgNPs are effective in inhibiting *E. coli* (Gram-negative) as well as *S. aureus* (Gram-positive), with 8 mm and 6 mm inhibition zones, respectively. Besides, *Cl*-AgNPs displayed a concentration-dependent antioxidant activity, suggesting ROS-mediated antibacterial activity. These findings highlight the anti-bacterial capability of these biogenic *Cl*-AgNPs.

Keywords: Green Synthesis, Silver Nanoparticles (AgNPs), *Curcuma longa* rhizome (*Cl*-rhizome), *Curcuma longa*-silver Nanoparticles (*Cl*-AgNPs), Antibacterial, Antioxidant, Reactive Oxygen Species (ROS)

***Correspondence:** mjiban@gmail.com

Citation: Amin DS, Banu AN, Mishra J. *Curcuma longa*-mediated Biogenic and Eco-friendly Silver Nanoparticles with Promising Antibacterial Activity. *J Pure Appl Microbiol.* 2026;20(1):622-641. doi: 10.22207/JPAM.20.1.48

INTRODUCTION

Nanotechnology has surfaced as a potential transformer of the healthcare by introducing advanced approaches to find alternative solutions to diagnose, treat, and prevent a plethora of maladies.[1] The surge in global prevalence of microbial diseases, together with the limitations of traditional therapeutics, has generated significant interest in metallic nanoparticles (NPs), especially AgNPs, for biomedical applications. These breakthroughs have not only enriched therapeutic strategies but also fostered innovations in targeted drug delivery and environmental remediation.[2] NPs are generally formed using two primary approaches: bottom-up and top-down. The top-down methodology necessitates employing physical processes to split up larger materials into a nanoscale structure, such as high-energy radiation and high-pressure techniques.[3] In the meantime, the bottom-up technique uses chemical and/or biological substances to put together nanomaterials from molecules or atoms. Various methods, involving the sol-gel process and chemical precipitation, are employed to regulate the configuration of nanoscale structures. While chemical synthesis is frequently used, it often creates hazardous by-products that pose harmful environmental threats. Biological synthesis, on the other hand, leverages natural resources like microbes and plants, which serve as reducing as well as stabilizing agents, synthesizing nanomaterials that are not very hazardous.[4,5]

AgNPs synthesized using environment-friendly methods are affordable, safe, minimally toxic, highly productive, cost-efficient, and easily accessible, making them a key candidate for developing novel therapeutic strategies suitable for applications in agriculture, biomedicine, and various other sectors.[6] Studies indicate that AgNPs are the most widely utilized metallic NPs, with an approximate worldwide production of around 500 tons per year for applications in medical devices, i.e., antimicrobial coatings, wound healing, surface modifications, textiles, water treatment, and purification systems.[7] AgNPs exhibit broad-spectrum antibacterial activity and possess antiseptic properties with minimal side effects, making them promising candidates for innovative therapeutic strategies. Their applications extend to drug delivery, water purification, and targeting antibiotic-resistant Gram-positive and Gram-negative bacteria.[8] Particularly, biofabricated AgNPs have gained significant attention due to their remarkable antibacterial and antioxidant properties. Studies indicate that AgNPs can traverse the cell membrane of *E. coli*, disrupt respiratory enzymes, generate reactive oxygen species (ROS), and severely impair bacterial cells by compromising the integrity of the cell wall. Despite their promising applications, the precise working principle of AgNPs, driven by the sustained release of silver ions, remains under investigation. This process ultimately results in bacterial cell death and degradation. The physicochemical properties of AgNPs, encompassing a high ratio of surface-area-to-volume, fervent catalytic activity, and variations in size and shape, contribute to their antibacterial efficacy.[9] However, despite extensive research, the precise mechanisms underlying their antibacterial action remain incompletely understood.[10-12] Plant-based methods, among various biosynthesis approaches, have gained prominence because of natural phytochemicals that enact as reducing as well as stabilizing agents. Plant extracts provide an effective strategy for the environment-friendly synthesis of AgNPs, owing to their abundant constituents of phytochemicals, encompassing both primary and secondary metabolites. These bioactive compounds behave as natural stabilizing and reducing agents, enabling the conversion of Ag^{+} to Ag° while ensuring NP stability.[13,14]

Curcuma longa (*Cl*), generally recognized as turmeric, has been thoroughly investigated for its medical benefits and has recognized to be a brilliant option for AgNPs biosynthesis. The biologically synthesized AgNPs using *Cl*-rhizome extracts enhance their stability and dispersion while imparting bioactive properties that improve their therapeutic efficacy.[15] The medicinal potential of the *Cl*-rhizome is primarily attributed to its rich composition of secondary metabolites, which have been traditionally utilized for treating various ailments, including inflammation and wound healing.[16] *Cl*, often known as the "Indian saffron" or "Golden spice", is a Zingiberaceae family member. It is popular for its vivid yellow-orange hue and unique flavor, rendering it a fundamental

component of South Asian cuisine. Besides its culinary importance, turmeric has diverse applications in other fields.[17,18] India considerably cultivates turmeric, accounting for around 80% of world production, whereas the United States of America is the leading importer.[19] The bioactive compound curcumin, a polyphenol extracted from the *Cl*-rhizome, exhibits diverse pharmacological properties. It possesses antibacterial, antiviral, anti-inflammatory, anticancer, neuroprotective, antidepressant, hepatoprotective, antiallergic, and antioxidant effects, making it a hot topic for significant scientific interest.[20,21]

The widespread preference for *Cl* from the Indian continent is largely attributed to its high curcumin content, which is the main bioactive molecule that gives it its healing properties. Curcumin has been considerably researched for its ability in averting and treating a variety of chronic conditions, comprising jaundice, ulcers, and liver disorders.[22] Furthermore, turmeric also exhibits strong anti-inflammatory and wound-healing qualities, which is advantageous for treating and managing ailments such as arthritis and intestinal disorders.[23]

Published literatures suggest that curcumin primarily exists in the β-keto-enol tautomeric form, exhibiting the keto form in aqueous environments and the enol form in organic solvents. Its molecular structure is influenced by pH levels.[24] Under acidic conditions, curcumin predominantly remains in its keto form, which contributes to its characteristic yellow colour.[21] Conversely, in alkaline conditions, it transitions to the enol form, which changes the colour from light-yellow to brownish-red.[25] This conversion occurs as the phenol hydroxyl (-OH) group interacts with the hydroxide ions (OH^-), leading to the formation of the phenoxide anion ($C_6H_5O^-$), which is generally visualized through the change in colour.[19,26] Recent research highlights the multifaceted applications of curcumin, including its role in cancer therapy, by changing the pathways that cells use to communicate, which are involved in tumor progression and metastasis. It has also demonstrated effectiveness in the management of various neurodegenerative diseases, like Parkinson's and Alzheimer's, by lessening oxidative damage and inflammation in neural tissues. Furthermore, when combined with pain medications, curcumin demonstrates synergistic effects in alleviating chronic pain while minimizing adverse side effects.[27] Beyond its therapeutic applications, curcumin contributes to skin health by combating aging-related factors, reducing wrinkles and pigmentation, and aiding in the treatment of acne and wound healing with its antibacterial and anti-inflammatory characteristics.[28] Additionally, curcumin serves as a natural food colorant and preservative, preventing microbial spoilage and potentially enhancing gut health and metabolic functions.[20] A recent study by Raduly et al. focused on developing advanced drug delivery systems to augment their bioavailability and clinical efficacy.[29] Moreover, curcumin's versatility extends across multiple domains, making it a valuable component in medicine, cosmetics, food science, and agriculture. Plant-based AgNPs are minimally toxic, eco-friendly, and cost-effective. They facilitate rapid synthesis without the need for external stabilizing agents and function under moderate conditions of temperature, pressure, and pH. This sustainable approach to NP synthesis enhances its biomedical potential in combating severe diseases while addressing concerns associated with conventional NP production.[30,31] Despite numerous reports on plant-mediated green synthesis of AgNPs, comprehensive studies utilizing *Cl*-rhizome extract that integrate optimization of synthesis conditions, detailed physicochemical characterization, and mechanistic investigation of antibacterial activity remain limited. Most previous works have not thoroughly explored how parameters like pH, precursor concentration, and extract-to-silver nitrate ($AgNO_3$) ratio influence nanoparticle formation and activity. Additionally, while *Cl* is rich in curcumin and other bioactive compounds, few studies have linked these phytochemicals to enhanced nanoparticle stability and ROS-mediated antimicrobial efficacy. This green-synthesis method favours the United Nations Sustainable Development Goals (UNSDGs), mainly SDG 3 (Good Health and Well-Being), SDG 6 (Clean Water and Sanitation), and SDG 12 (Responsible Consumption and Production), by promoting eco-friendly NP production with antimicrobial potential.

This investigation intends to bridge the scientific gap by optimizing the synthesis of

Cl-AgNPs under varied physicochemical conditions, conducting multi-technique characterization, and assessing their antibacterial mechanism through ROS generation. The novelty of our approach lies in demonstrating the superior biomedical potential of *Cl*-AgNPs, especially inhibiting *E. coli* and *S. aureus* bacterial infections while contributing a scalable and environmentally friendly alternative for chemically synthesized NPs in nanomedicine and antimicrobial therapeutics.

The biological method of AgNP synthesis using *Cl*- extract can compete with, and, in some applications, even surpass, conventional chemical and physical synthesis methods, provided it is optimized, standardized, and scaled properly. This approach is a long-lasting, sustainable, and biocompatible alternative to the traditional methods. While it provides environmental and cost advantages, its market competitiveness depends on addressing challenges related to standardization, scalability, and regulatory compliance. With ongoing advances in green nanotechnology and extract optimization, *Cl*-AgNP synthesis holds strong promise for usages in antimicrobial, biomedical, and environmental fields.[32]

MATERIALS AND METHODS

MATERIALS

The chemicals, reagents, media used were of analytical grade, including $AgNO_3$ (Loba Chemie Pvt. Ltd., 99.9% AR/ACS), sodium hydroxide (NaOH, Rankem AR/ACS), and 2,2-diphenyl-1-picrylhydrazyl (DPPH) (Loba Chemie Pvt. Ltd.). Ascorbic acid and agar media (Luria-Bertani broth and agar), Gram-negative bacteria *E. coli* (MTCC 1698), Gram-positive bacteria *S. aureus* (MTCC 3160), and *E. coli* DH5α obtained from Himedia Laboratories Pvt. Ltd. All the glassware was rinsed with Aqua-Regia in the ratio of 3:1, followed by cleaning with Milli-Q water. Organically grown *Curcuma longa* (*Cl*) rhizome was used in this study.

METHODS

Collection and identification of *Cl*-rhizome

The organically grown rhizome of the *Cl* was collected from the herbal garden at Lovely Professional University, Phagwara, Punjab, India. Its identity was authenticated at the Indian Institute of Integrated Medicine (CSIR-IIIM, Jammu, India) and assigned a herbarium accession number (RRLH-24809). The collected rhizome was properly cleaned with distilled water, dried using a tray dryer, crushed and sieved into fine powder, and stored in an airtight bottle for subsequent experiments.

Preparation of aqueous extract of *Cl*-rhizome

The aqueous extract of the *Cl*-rhizome was prepared as per the methodology reported previously,[33] with certain changes. To prepare the extract, 2 g of plant rhizome powder was added to a flask containing 100 ml of MilliQ water. The mixture was further heated for 10-15 min. at 80-90 °C, yielding a dark yellow solution. Upon cooling, the solution was filtered using Whatman No. 1 filter paper, and the plant extract was preserved at 2-4 °C for subsequent use.

Synthesis of AgNPs

The green synthesized *Cl*-AgNPs were standardized under desirable conditions to improve accuracy, utilizing an extract to $AgNO_3$ ratio of 1:9, a pH of 12, room temperature (RT), and a reaction duration of 24 hrs. This procedure efficiently achieved stable NP formation in several replicates, as verified by UV-vis and DLS analysis. The *Cl*-rhizome prepared with Milli Q water was gently added to the aqueous $AgNO_3$ (1 mM) solution in a ratio of 1:9 dropwise and to initiate the reduction of Ag^+ ions to Ag°. Avoiding photochemical deterioration, the reaction mixture was maintained at RT in the absence of light. The colour of the *Cl*-AgNPs shifted from light-yellow to brownish-red, depicting the manufacture of AgNPs. The resultant reaction mixture solution was further centrifuged at 10,000 rpm for 40 min. to pellet down the *Cl*-AgNPs, which were then thoroughly washed with Milli Q water to eliminate unbound phytochemicals. The washed pellet was further dried in a hot air oven maintained at 40-50 °C and stored for later characterization, as illustrated in Figure 1.

While *Cl*-rhizome extract works as a green stabilizing, reducing, and capping agent, unreacted organic compounds or impurities in the extract may influence NP stability and biological activity. To minimize these effects, synthesized *Cl*-AgNPs were purified via centrifugation and washing

with distilled water. Nonetheless, future work will include advanced purification and cytotoxicity testing to evaluate the effect of residual waste on biocompatibility and storage stability.

Optimization parameters of *Cl*-AgNPs

Different parameters influencing the synthesis of *Cl*-AgNPs were optimized, i.e. the plant extract-$AgNO_3$ ratio, concentration of $AgNO_3$, pH of the *Cl*-AgNPs, and reaction time. To standardize the optimal condition for efficient synthesis of *Cl*-AgNPs, different precursor concentrations (1-5 mM), plant extract-to-precursor ratios (1:1, 1:2, 1:5, and 1:9), and pH (ranging from 6-12) were evaluated. All experiments were conducted in triplicate and under dark conditions to prevent any light-induced reactions.

The synthesized *Cl*-AgNPs extracted from *Cl*-rhizome in this experiment were consistent, as shown by reproducible SPR peaks, stable zeta potential, and particle morphology across batches. However, plant-based synthesis inherently depends on the phytochemical composition of the extract, which can vary. Therefore, extract preparation conditions were carefully controlled to maintain reliability.

Characterization of *Cl*-AgNPs

The bio-fabricated *Cl*-AgNPs were analysed with different techniques to uncover their optical, structural, and morphological properties. UV-vis. analysis was achieved using a Lasany/Shimadzu spectrophotometer (Model No. LI-2800) to monitor the SPR and confirm NPs formation. The reduction rate was confirmed by recording the SPR peak at regular intervals, and the reaction was considered complete once the peak intensity at 423 nm stabilized after approximately 24 h, indicating saturation in NP synthesis. Structural characterization was conducted using XRD, utilizing a Bruker D8 Advance diffractometer to ascertain the crystalline nature. Functional group analysis was confirmed using FTIR on a Perkin Elmer Spectrum 2 instrument to identify biomolecules involved in reduction and capping. Morphological and structural assessments were performed utilizing TEM using a JEOL TEM 2100 Plus and SEM using a JEOL SEM-JSM 7610F, both complemented by EDAX for elemental composition analysis. Additionally, DLS analysis was conducted with a Malvern Zetasizer Nano ZS 90 to assess zeta size and zeta potential, providing insights into the dispersion stability and surface charge of the NPs.

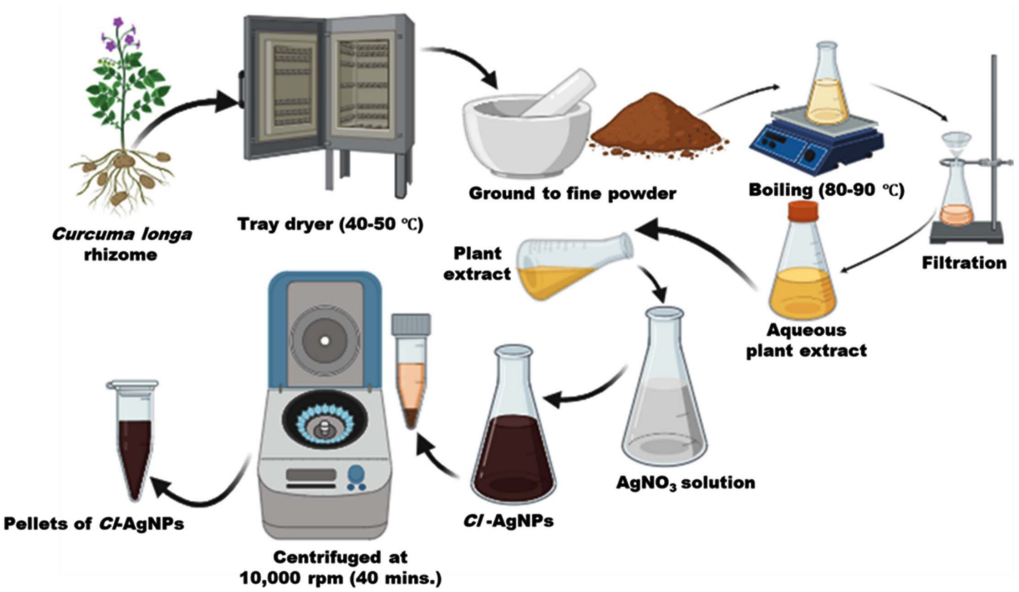

Figure 1. Schematic representation of *Cl*-AgNPs synthesis by the green synthesis method

Antioxidant efficiency of *Cl*-AgNPs

The antioxidant radical scavenging capacity of *Cl*-rhizome extracts and *Cl*-AgNPs was assessed using the DPPH assay. Different concentrations (200, 400, 600, 800, and 1000 µg/ml) of *Cl*-AgNPs, *Cl*-rhizome extract, and ascorbic acid as a reference standard were used. Each test sample was individually added in a 1:1 ml ratio of DPPH with extract and AgNPs, and was kept for 30 min. in the dark at 37 °C. The absorbance (517 nm) was recorded using a spectrophotometer. Methanol served as the blank, while ascorbic acid included as the positive control.[34,35] The free radical scavenging activity (%) was calculated using Equation (1).

$$\text{DPPH activity (\%)} = [\text{Abs(Control)} - \text{Abs (test sample)} / \text{Abs(Control)}] \times 100 \quad ...(1)$$

Where, Abs is the absorption

A graph was plotted to illustrate the scavenging efficiency at different sample concentrations. The experimental setup was performed in triplicate (n = 3), and results were noted as mean ± SD. One-way ANOVA followed by Duncan's post-hoc analysis was used to find the significant differences between the experimental groups.

Antibacterial application of *Cl*-AgNPs
Well-diffusion method

The bactericidal properties of *Cl*-AgNPs were determined against *E. coli* and *S. aureus* using the well-diffusion method, in accordance with the Clinical and Laboratory Standards Institute (CLSI) protocols, and the method was adapted with modifications by Ahmed et al.[36] In this assay, the glycerol stock of the bacterial cultures was revived in sterilized broth of Luria-Bertani (LB) and incubated for 24 h, at 37 °C. The following day, 100 µl of the freshly revived inoculum was uniformly spread onto Nutrient Agar (NA) plates through a sterile glass spreader. Five wells were aseptically bored into the agar using a sterile borer with each well supplemented with 100 µl from a 1 mg/ml stock solution of each sample, including *Cl*-AgNPs, a positive control (streptomycin), a negative control (deionized water), *Cl*-rhizome extract, and $AgNO_3$ as a precursor. The plates underwent incubation for another 24 hrs, at 37 °C, after which the zone of inhibition was calculated using a slide calliper, and the measurements were expressed in millimeters (mm).[37]

Minimum Inhibitory Concentration (MIC)

The broth dilution technique was used to reveal the MIC of *Cl*-AgNPs for *E. coli* and *S. aureus*. *Cl*-AgNPs were added to fresh bacterial cultures at concentrations of 50, 100, 150, and 200 µg/ml. The MIC for *E. coli* was observed to be 100 µg/ml, since observable growth was completely inhibited at this concentration. Compared to *Cl*-AgNPs, *S. aureus* had a lesser sensitivity with a MIC of 150 µg/ml. These findings suggest that *E. coli* is more prone to synthesized NPs than *S. aureus*, probably due to cell wall differences.[38]

Minimum Bacterial Concentration (MBC)

To evaluate the MBC, aliquots from the MIC tubes were inoculated onto LB agar plates enriched with the respective concentrations of *Cl*-AgNPs. Bacterial growth was checked post-incubation of 24 hrs. The MBC for *E. coli* was around 150 µg/ml; however, *S. aureus* requires a higher concentration of approximately 200 µg/ml to attain 90% of bacterial death. These findings further validate the greater efficacy of *Cl*-AgNPs against *E. coli* in comparison to *S. aureus*.

The enhanced sensitivity of *E. coli* can be attributed to the weakened peptidoglycan layer and the outer membrane of the cell structure, which facilitates more facile penetration and interaction with AgNPs. However, the thicker peptidoglycan protective layer of Gram-positive bacteria, such as *S. aureus,* might block penetration of NPs, which led to the higher dosage for efficient bacterial activity. This outcome is consistent with prior research studies about the varied sensitivity of bacterial strains to *Cl*-AgNPs.

Reactive Oxygen Species (ROS)-mediated antibacterial mechanism

The DCFDA test was utilized to evaluate intracellular ROS generation in *E. coli* subsequent to treatment with *Cl*-AgNPs. The mechanism of antibacterial application indicates oxidative stress, which plays a pivotal role and leads to the emergence of green fluorescence in the

treatment of bacterial cells, which signifies increased ROS levels. Nonetheless, it is essential to acknowledge that this experiment yielded only qualitative evidence of ROS generation. Quantitative fluorescence intensity measurements using a microplate reader or flow cytometer were not performed due to instrumentation constraints. Future studies should incorporate quantitative ROS analysis to strengthen the mechanistic understanding of *Cl*-AgNP-induced bactericidal activity.

Detection of ROS

The impact of *Cl*-AgNPs on the accumulation of ROS in bacterial cells was assessed using 2',7'-dichlorofluorescein diacetate (DCFDA), a fluorogenic dye that detects hydroxyl radicals, peroxyl radicals, and other activities of ROS.[39] Bacterial cultures were subjected to *Cl*-AgNPs and adjusted to a concentration of 1×10^6 cells/ml, while untreated samples served as controls. All cultures were maintained for 24 hrs at 37 °C. Post-incubation, the bacterial cells were centrifuged at 6000 rpm for 10 min., and the supernatant was removed. The pellets were then resuspended in 100 µM DCFDA and incubated in dark for 1 hr, followed by washing with 1× PBS. All experiments were repeated thrice, and fluorescence imaging was performed using a ZEISS confocal laser imaging microscope.

RESULTS AND DISCUSSION

The green-synthesis of *Cl*-AgNPs was evidenced by a significant change in colour of the reaction mixture, which shifted from yellowish to brownish-red at RT due to SPR. After 24 hrs, the reaction mixture further transitioned from light brown to brownish-red, confirming the reduction of Ag^+ to Ag°.

Optimization of Parameters for the Synthesis of *Cl*-AgNPs

Precursor concentration

Among the various precursor concentrations (1-5 mM) tested, 1 mM was found

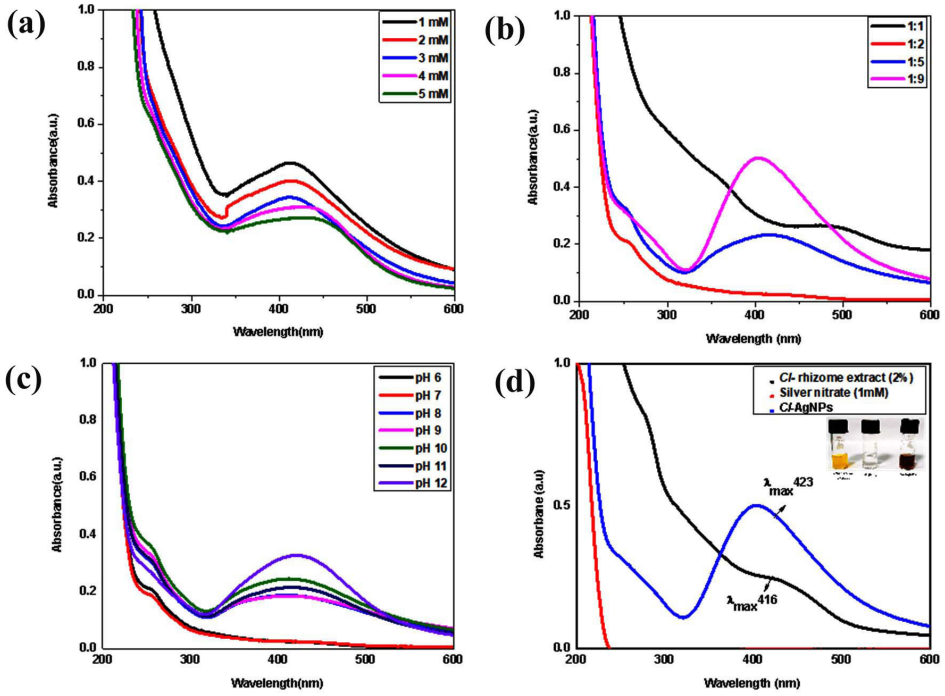

Figure 2. Synthesis of *Cl*-AgNPs using the standardized conditions: (a) Precursor concentration (1-5 mM), (b) Plant extract-precursor ratio graph of *Cl*-AgNPs with different ratios, (c) UV-Vis graph of *Cl*-AgNPs showing absorbance at different pH, (d) UV-Vis graph of *Cl*-rhizome extract (2%), $AgNO_3$ (1 mM), and *Cl*-AgNPs

to be optimal for the nano-scaling of $AgNO_3$. It was noted that elevated precursor concentrations resulted in a lower yield of AgNPs. UV-vis analysis (Figure 2a) showed a decline in absorbance with increasing precursor concentration. Therefore, 1 mM was selected as the ideal concentration, as it produced a sharp and well-defined SPR peak at 400 nm, signifying efficient AgNP synthesis.

Plant extract-precursor ratio

A freshly prepared aqueous extract of *Cl*-rhizome powder was used to reduce Ag^+ ions to Ag°, with varying volume ratios of *Cl*-rhizome extract to $AgNO_3$ (1:1, 1:2, 1:5, and 1:9), as shown in Figure 2b. Among these, the 1:9 ratio confirmed the successful formation of *Cl*-AgNPs. These results suggest that increasing the proportion of the precursor in the reaction mixture enhances the efficiency of AgNP synthesis compared to lower $AgNO_3$ concentrations.

pH

pH plays a crucial role in NPs synthesis, influencing their size, morphology, and stability. Research indicates that higher pH levels in the solution generally give rise to the formation of smaller NPs and speed up the synthesis process.[40,41] To find out the optimal pH for fabricating AgNPs, the pH of reaction mixture was adjusted between 6 and 12. At pH 6, the aqueous reaction mixture exhibited a light-yellow hue, while at pH 12, it transitioned to a reddish-brown colour. Notably, at pH 12, the *Cl*-AgNPs were predominantly spherical and demonstrated the highest absorbance peak compared to those synthesized at pH 10 and pH 11. Further, Joshi et al.[42] reported that an alkaline pH environment enhances AgNP synthesis by promoting greater stability, higher yield, and an improved reduction process. Additionally, variations in the intensity of the reaction mixture's colour with a change in pH, as depicted in Figure 2c, further confirm these observations. Based on the spectral analysis, pH 12 was found to be the optimal condition for synthesizing *Cl*-AgNPs quickly and easily.

Synthesis of *Cl*-AgNPs at standardized conditions

Based on the optimization experiments, the ideal conditions for *Cl*-AgNP synthesis were established as follows: a precursor concentration of 1 mM, a 1:9 ratio of plant extract to precursor, and a pH of 12. Under these optimized parameters, the synthesis of *Cl*-AgNPs occurred instantly at RT and was subsequently characterized using various analytical techniques. The corresponding spectrum, presented in Figure 2d, shows a strong peak at 423 nm, which represents the SPR of *Cl*-AgNPs.

Characterization of *Cl*-AgNPs

UV-vis Spectroscopy

The UV-vis spectroscopy of *Cl*-rhizome extract exhibited a peak absorbance observed at λ_{max} 416 nm, which shifted to λ_{max} 423 nm upon the formation of *Cl*-AgNPs (Figure 3a). When *Cl*-rhizome extract is dissolved in water, the curcumin molecules absorb light in the blue-violet spectrum, making the solution appear yellow.[43] In this study, the dropwise addition of *Cl*-rhizome extract to a solution of $AgNO_3$ led to a visible change in colour from light yellow to brownish-red at RT, with a changing pH of the solution. This transformation is attributed to SPR, NP aggregation, particle size, interactions with other compounds, and variations in the dielectric environment.[44,45] Previously published literature has shown that curcumin exhibits a pH-dependent colour transition between pH 2 and 13. It remains yellow in acidic to neutral conditions (pH 2-7) but shifts to a brownish-red hue in alkaline environments (pH 8-13). The addition of 0.1N NaOH effectively ionizes curcumin crystals, enhancing their solubility.[46] The optical studies confirmed *Cl*-AgNPs synthesis with a significant peak within the 400-430 nm range, indicative of AgNP formation.[47] Post 24 hrs, the reduction of Ag^+ to Ag° resulted in the change in colour of the solution from light brown to reddish-brown. Furthermore, this colour variation is closely linked to the morphology (shape and size) of the *Cl*-AgNPs, as well as pH fluctuations, which influence their morphological and optical properties. The *Cl*-rhizome extract serves as both a stabilizer and a reducing agent, facilitating the controlled size and leading to the synthesis of smaller AgNPs.[48]

Higher temperatures can accelerate NP aggregation by detaching the capping agents that don't require high temperatures or induce morphological changes by disrupting the capping biomolecules, changing the NP shape due to

increased kinetic energy. While exposure to light, especially UV-vis. can also induce photoactivation, leading to potential oxidative degradation or surface modification, altering their properties. Similarly, extreme pH conditions modify the ionization or deionization of the functional groups on the NP surface, which affects their colloidal stability and zeta potential.[49]

XRD

XRD is a highly effective analytical technique, enabling both qualitative and quantitative analysis of the crystal structure and degree of crystallinity. The XRD diffractogram of *Cl*-AgNPs showed distinct peaks at 2θ values of 23°, 27°, 32°, 38°, 46°, 54°, 57°, and 76°, corresponding to the (111), (200), (220), and (311) planes of AgNPs, as depicted in Figure 3b. The crystal size calculated by the equation of Debye–Scherrer is smaller (~16 nm) than the TEM-derived particle size (~47.6 nm), which can be attributed to the fact that XRD measures individual crystalline domains, whereas TEM captures the entire NP, including aggregated or polycrystalline structures. The observed crystallite size and peak intensities correspond with those documented for plant-derived AgNPs synthesized via green methods in prior research.[50,51]

The crystal size of *Cl*-AgNPs was calculated using the equation of Debye-Scherrer, which is given as:

$$D = k\lambda/\beta \cos \theta \quad \text{...Equation (2)}$$

Where, D = Crystallite domain size, k is the Scherrer's constant (k = 0.94), λ = X-ray wavelength (1.540 + Å), β is the full width at half maximum (FWHM), and θ is the angle of diffraction. Using Equation (2), the synthesized *Cl*-AgNPs exhibited an average crystallite size of ~16 nm, which aligns with the FCC structure of AgNPs.

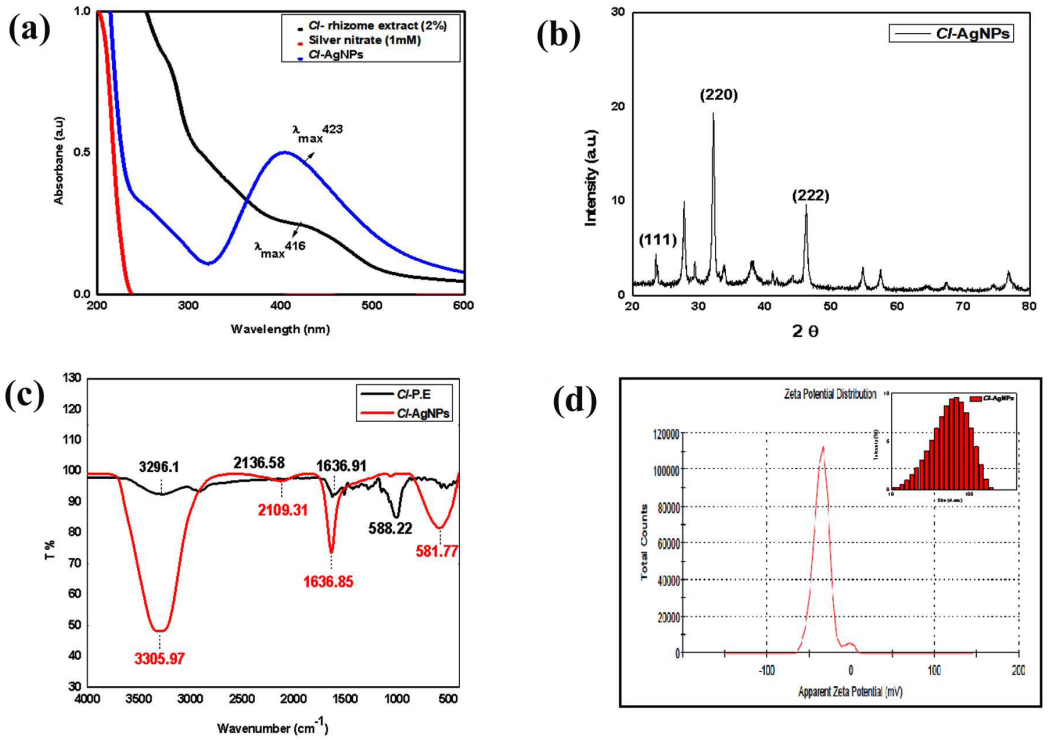

Figure 3. Analysis of *Cl*-AgNPs: (a) UV-Vis graph shows *Cl*-rhizome extract, $AgNO_3$, and *Cl*-AgNPs, (b) XRD peaks confirm the fcc crystalline nature of *Cl*-AgNPs, (c) FTIR graph of *Cl*-rhizome extract and *Cl*-AgNPs, (d) DLS histogram of *Cl*-AgNPs showing Zeta size and Zeta potential values indicating the stability of *Cl*-AgNPs

FTIR

FTIR analysis was performed to identify the active functional groups responsible for the bio-fabrication of AgNPs. The spectra of the *Cl*-rhizome extract and the synthesized *Cl*-AgNPs were recorded in the 400-4000 cm^{-1} range. The FTIR peaks of the *Cl*-rhizome extract were observed at 3296.1, 2136.58, 1636.91, and 588.22 cm^{-1}, corresponding to O-H stretching, C-H stretching, C=O stretching, and Ag-O bonds, respectively. In contrast, the FTIR spectrum of *Cl*-AgNPs displayed slight shifts in the corresponding peaks to 3305.97, 2109.31, 1636.85, and 581.77 cm^{-1}.[8,41] These shifts indicate the involvement of various functional groups that are involved in stabilizing and reducing AgNPs. For example, the shift from 2136.58 cm^{-1} to 2109.31 cm^{-1} reflects interaction between the bioactive compounds in the extract and Ag^+ during NP formation. Similarly, the shift in the Ag-O region suggests molecular interaction and binding during the reduction process. The participation of hydroxyl groups under alkaline conditions further enhances the reduction process and stabilizes the NPs.[37,52] *Cl* extract is rich in curcumin, which contains (-OH) and β-diketone functional groups capable of donating electrons to reduce Ag^+ ions to elemental silver (Ag°). The electrons initiate the process of nucleation and formation of AgNPs. Additionally, *Curcuma* extract comprises an extensive range of phytoconstituents, including tannins, flavonoids, alkaloids, glycosides, and terpenoids, many of which possess hydroxyl and carbonyl groups that help reduce Ag^+ and stabilize the resulting NPs by capping their surfaces. The

Table. Showing the proportion of elements present in the synthesized *Cl*-AgNPs formed from the extract of *Cl*-rhizome: Spectrum 1 = Elements present; (wt%) = normalized weight percent of the element; (wt% sigma) = the atomic weight percent; error in the weight percent concentration

Spectrum 1	Wt%	Wt% Sigma
C	16.34	0.46
O	25.70	0.71
Na	2.04	0.20
Ag	55.92	0.67
Total	100.00	

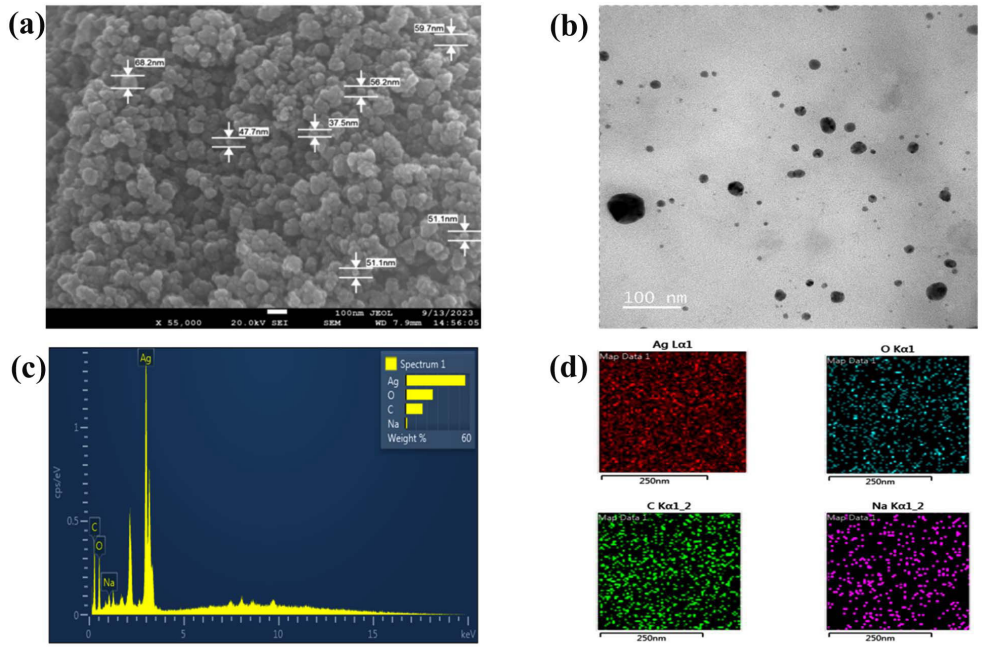

Figure 4. (a) SEM image of *Cl*-AgNPs revealed spherical shape observed under 50,000x magnification at 100 nm, (b) HR-TEM image of *Cl*-AgNPs by drop cast method at 100 nm, (c) Elemental detection analysis of *Cl*-AgNPs indicating the existence of Ag^+ at 3 KeV, (d) Silver (red colour) in *Cl*-AgNPs at 250 nm in elemental mapping, indicating successful coating

FTIR analysis further supports this mechanism by confirming the presence and involvement of these functional groups, thereby validating the dual activity of *Cl*-rhizome extract as both a reducing and capping agent.[53]

DLS

The DLS technique was employed to find out the hydrodynamic diameter, PDI, and Zeta size and potential of the *Cl*-AgNPs. As shown in the DLS histogram (Figure 3d), the hydrodynamic diameter of the *Cl*-AgNPs was found to be ~42.98 nm, with a PDI of 0.554, suggesting a moderate size distribution.[54] Additionally, the DLS analysis revealed a sharp unimodal peak centered around ~58.61 nm, reflecting a monodispersed population of NPs. In a colloidal state, the sharpness of the peak indicates uniform particle size and effective surface capping, which contribute to the stability of AgNPs synthesis. The negative zeta potential of

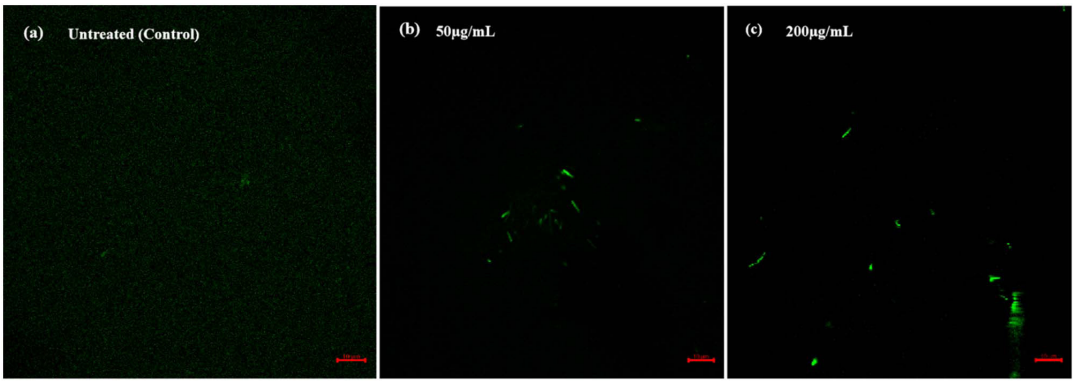

Figure 5. *Cl*-AgNPs induced cellular ROS generation: (a) Untreated control, (b) *Cl*-AgNPs treated *E. coli* DH5α at 50 µg/ml concentration, (c) *Cl*-AgNPs treated *E. coli* DH5α strain at 200 µg/ml concentration

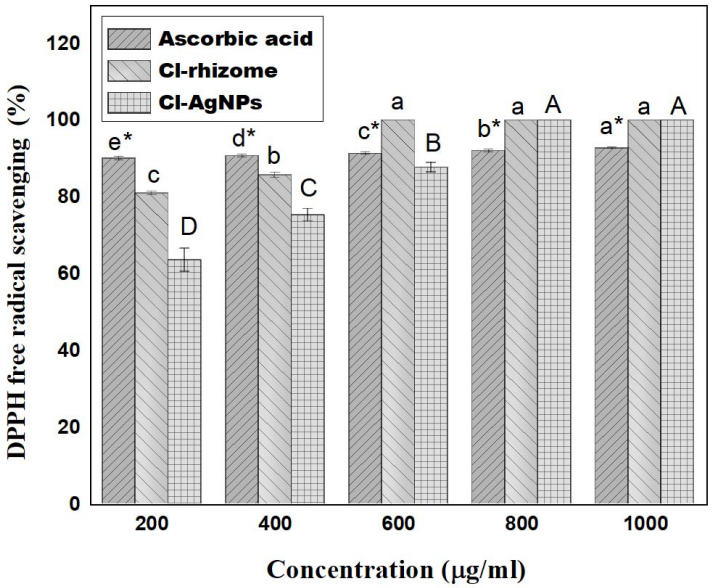

Figure 6. DPPH radical scavenging assay of *Cl*-rhizome, Ascorbic acid, and *Cl*-AgNPs at different dosages (200, 400, 600, 800, and 1000 µg/ml) showed mean ± SD of triplicate measurements (n = 3) for antioxidant activity. Lowercase (a, b, c); uppercase (A, B, C, D) and lowercase with asterisks (a*, b*, c*, d*, and e*) indicate significant differences between groups as determined by Duncan's multiple range post-hoc test ($P < 0.05$). Values with the same letters are not significantly different from each other

the *Cl*-AgNPs, indicating a highly negative charge of the surface, was measured at -32.4 mV. This strong electrostatic repulsion between particles plays a crucial role in preventing aggregation, thereby enhancing long-term dispersion stability.[55]

Previous studies have reported comparable zeta potential values for AgNPs synthesized from medicinal plants such as *Potentilla fulgens* (-18 mV), *Alpinia calcarata* (-19 mV), *Pestalotiopsis microspora* (-35.7 mV), *Urtica dioica* (-24.1 mV),

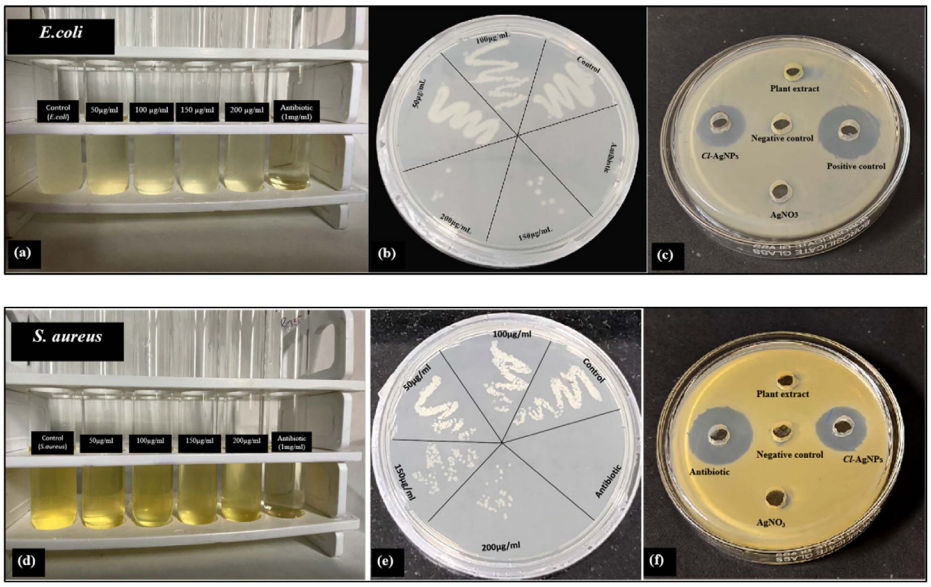

Figure 7. Efficacy of *Cl*-AgNPs against *E. coli* and *S. aureus* strains. (a) and (d) MIC of *Cl*-AgNPs with varying dosage (50, 100, 150 and 200 µg/ml) depicting MIC values at 200 µg/ml (low turbidity), (b) and (c) are MBC results obtained from test tubes of MIC with different concentration of *Cl*-AgNPs, (e) and (f) Well-diffusion method of *Cl*-AgNPs, Plant extract, Positive control (Streptomycin), and negative control (Deionized water), all at dosage of 1 mg/ml

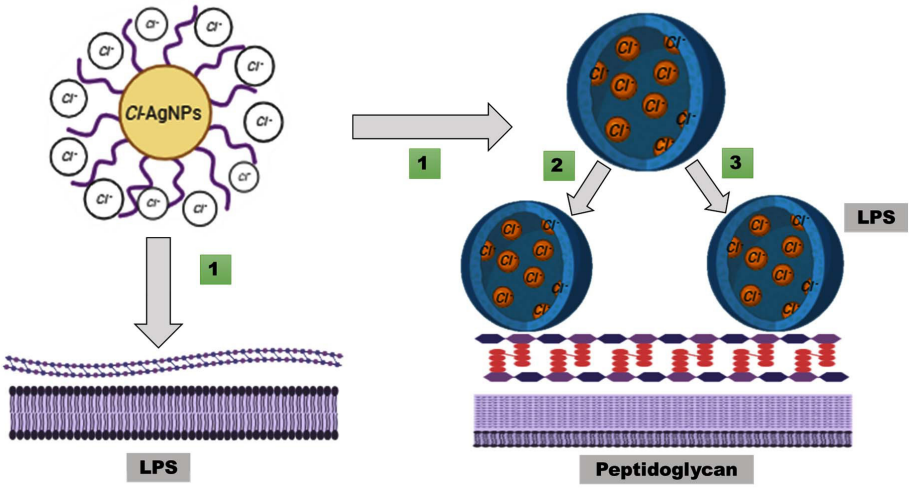

Figure 8. Schematic representation of the interaction between *Cl*-AgNPs and bacterial cell wall components. (1) *Cl*-AgNPs approach the bacterial surface and initially interact with lipopolysaccharides (LPS) in *E. coli*, (2) *Cl*-AgNPs adhere to the external surface of the peptidoglycan protective layer in *S. aureus*, disrupting cell wall integrity. (3) In *E. coli*, after LPS interaction, *Cl*-AgNPs penetrate and interact with the underlying peptidoglycan layer, enhancing antimicrobial activity through ROS generation and membrane destabilization

and *Jatropha curcas* (-23.4 mV), which align well with our findings. In general, NPs with zeta potential values exceeding ± 30 mV are considered stable in suspension. Thus, the zeta potential of *Cl*-AgNPs observed in this study supports their excellent colloidal stability and confirms consistency with previously reported literature.[41,56,57]

SEM

The morphological and topographical characteristics were studied by SEM analysis for *Cl*-AgNPs. The *Cl*-AgNPs found to be spherical, a highly desirable trait for various applications. SEM measurements indicated that the synthesized *Cl*-AgNPs ranged in size between 30 and 70 nm, as depicted in Figure 4a. These results correspond to the previous studies, including those by Gupta et al,[58] which reported spherical AgNPs ranging from 37.2 to 65.1 nm in curcumin-based wound healing applications. Similarly, biosynthesized AgNPs derived from an aqueous extract of the *Cl*-rhizome exhibited comparable characteristics.[8,41] Other research further supports these findings, with studies on plant-mediated AgNP synthesis reporting similar results. For instance, AgNPs synthesized from *Cuphea carthagenensis* extract ranged from 4-18 nm and were spherical, while those derived from *Piper retrofractum* extract ranged from 13.85-34.30 nm, maintaining their spherical morphology.[17,18] The size range of *Cl*-AgNPs in the SEM analysis is a crucial factor since reduced size of NPs usually have higher surface area to volume ratios, which makes them more reactive and also have unique physicochemical properties. SEM micrographs revealed predominantly spherical NPs with relatively smooth surfaces and minimal signs of aggregation. The well-dispersed appearance supports the hypothesis that bioactive compounds in the *Cl* extract effectively stabilized the NPs. These analytical techniques make them exceedingly useful for biological use, such as drug delivery and antimicrobial activity.[17,59]

HR-TEM

A solution of *Cl*-AgNPs was deposited onto a copper grid coated with carbon. For sample preparation, a diluted solution of *Cl*-AgNPs was utilized to prepare the samples. After the drying process, the samples were air-dried at RT and subsequently placed in a desiccator before analysis. The HR-TEM picture, which is displayed in Figure 4b, showed that *Cl*-AgNPs are spherical in shape. Using ImageJ software to analyze TEM images, *Cl*-AgNPs had an average particle size of 47.6 ± 8.2 nm, with maximum particles exhibiting spherical morphology. This size range is consistent with the DLS and XRD data. The spherical *Cl*-AgNPs formed via plant-mediated approaches are well documented with the results of prior research studies.[17]

EDAX with elemental mapping

The elemental composition of *Cl*-AgNPs and quantitative analysis were characterised by using the EDAX. A prominent absorption peak corresponding to elemental silver was observed at 3 keV, as depicted in Figures 4c and 4d. The EDAX graph depicts the presence of carbon (C), oxygen (O), sodium (Na), and silver (Ag) in the powdered sample, with their respective proportions of 16.34%, 25.70%, 2.04%, and 55.92%, as detailed in Table. These results confirm the effective synthesis of *Cl*-AgNPs and provide insight into their elemental composition.

Detection of ROS by DCFDA (2',7'-dichlorofluorescin diacetate) method in bacterial cells

Various studies have demonstrated that AgNPs significantly boost intracellular ROS generation, which subsequently inflicts damage on essential components of cells, including lipids, proteins, and DNA. The DCFDA assay is widely used to quantify ROS levels in bacterial cells exposed to AgNPs, as previously reported Bera et al and Karanam & Arumugam.[60,61] In this method, the fluorescence emitted by DCF serves as a reliable marker of ROS presence within cells, providing valuable insights into the extent of oxidative stress induced by AgNPs, as shown in Figures 5a, 5b, and 5c.

In the present study, *Cl*-AgNPs were shown to cause oxidative stress in bacterial cells by generating ROS, compared to the untreated control, ultimately leading to bacterial cell death. This oxidative stress is primarily attributed to the interaction of AgNPs with the bacterial cell wall, which disrupts cellular processes and triggers ROS production. These findings further support

the antimicrobial potential of *Cl*-AgNPs governed through a ROS-mediated mechanism.

Antioxidant activity

Cl is well known for its strong antioxidant properties.[35,62] In this study, *Cl*-AgNPs exhibited significant antioxidant potential, which is attributed to various phytoconstituents found in the *Cl*-rhizome extract, such as alkaloids, flavonoids, and the primary bioactive compound curcumin. The antioxidant activity of the *Cl*-rhizome extract, *Cl*-AgNPs, and ascorbic acid was found to be concentration-dependent, increasing with dosage. Notably, *Cl*-AgNPs demonstrated superior antioxidant efficacy compared to ascorbic acid (the standard), as illustrated in Figure 6. Furthermore, *Cl*-AgNPs displayed significant DPPH radical scavenging activity, underscoring their potential applications in the medical field.

The antioxidant potential was measured using the assay of DPPH, in which *Cl*-AgNPs, *Cl*-rhizome extract, and ascorbic acid were incubated with the solution of DPPH, then the absorbance after 30 min was measured at 517 nm. The plotted scavenging data (Figure 6) indicate that all tested samples exhibited more than 50% scavenging at 200 µg/ml, suggesting that the IC_{50} values are below 200 µg/ml. Specifically, *Cl*-AgNPs exhibited an IC_{50} around 130-160 µg/ml, which is less than that of the *Cl*-rhizome extract and close to that of ascorbic acid. All IC_{50} estimates were normalized to µg/ml and conducted in triplicate.

The antioxidant test findings were shown as the mean ± SD for each treatment group.

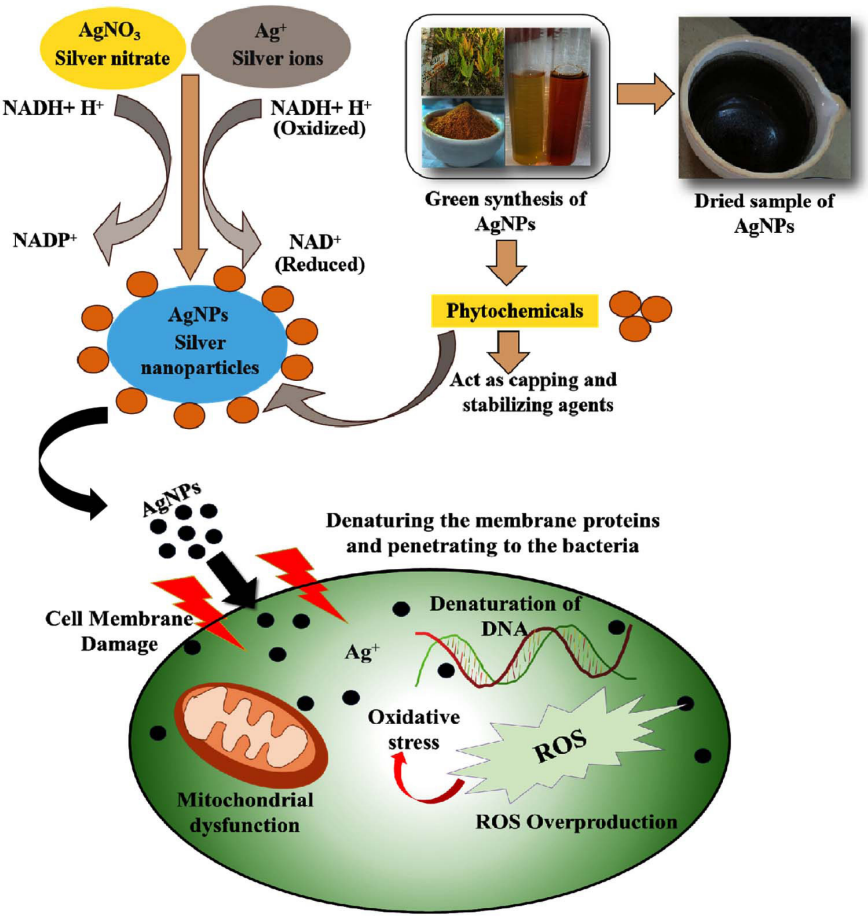

Figure 9. Diagrammatic illustration of the antibacterial mechanisms of action of AgNPs involving multiple pathways

Statistical analysis was performed by employing one-way ANOVA, followed by Duncan's post-hoc test, with a significance threshold of $p < 0.05$. In the graphical representation, distinct letters indicate significant differences: lowercase letters (a, b, c) correspond to variations in the *Cl*-rhizome extract, uppercase letters (A, B, C) represent differences in *Cl*-AgNPs at varying concentrations, and lowercase with asterisks (a*, b*, c*, d*, e*) denote significant differences in the ascorbic acid (standard sample) group at $p < 0.05$.

Bactericidal activity

The antibacterial assay of *Cl*-AgNPs was performed through well-diffusion method utilizing *E. coli* and *S. aureus* species. Initially, glycerol stocks of bacterial cultures were revived in Luria-Bertani (LB) broth and incubated for 24 hrs at 37 °C in an incubator shaker. The next day, each Nutrient Agar (NA) plate was added with 100 µl of the revived bacterial inoculum and uniformly spread over the surface of the plate using a sterile glass spreader. Five wells were aseptically made in the agar using a sterile borer. Each well was added with 100 µl of *Cl*-AgNPs, antibiotic, as a positive control (streptomycin), a negative control (deionized water), $AgNO_3$ as the metal ion solution, and *Cl*-rhizome extract, all at a dosage of 1 mg/ml. The prepared NA agar plates with treated samples were then incubated for 24 hrs at 37 °C. Post-incubation, zone of inhibition was measured in millimeters (mm) using a slide calliper and documented, as shown in Figures 7a-f.

The efficacy of *Cl*-AgNPs was confirmed against the bacterial strains utilizing MIC, MBC, and well-diffusion techniques. All MIC and MBC assays were performed using LB broth (pH 7.4) under sterile conditions. NP stock solutions were freshly prepared and used immediately.

The results showed that *Cl*-AgNPs exhibited a better and stronger inhibitory effect against *E. coli*, with an MIC of 100 µg/ml and an MBC of 150 µg/ml, as compared to *S. aureus*, which displayed an MIC of 150 µg/ml and an MBC of 200 µg/ml. These findings demonstrate a higher susceptibility of *E. coli* to *Cl*-AgNPs, consistent with earlier studies on AgNPs synthesized via green methods. This difference in bacterial sensitivity can be ascribed to the structural attributes of their distinct cell walls.

E. coli has a weaker peptidoglycan protective layer and an external membrane that is rich in lipopolysaccharides. This may make it easier for NPs to get through and interact with them. In contrast, *S. aureus* has a thicker or stronger peptidoglycan layer, which probably functions as a physical barrier, reducing AgNP penetration and requiring a higher NP concentration to achieve bactericidal effects, as illustrated in Figure 8.

A comparative analysis with reported literature highlights the enhanced antibacterial effectiveness of AgNPs synthesized using *Cl*-rhizome extract. In a study by Ahmed et al., synthesized AgNPs using *Azadirachta indica* showed an inhibition zone at 9 mm for both *E. coli* and *S. aureus*, with MIC of 100-150 µg/ml and an MBC of 200 µg/ml. Similarly, Sathyavathi et al. reported AgNPs derived from *Coriandrum sativum* that exhibited inhibition zones of 6-10 mm against *E. coli* and *Bacillus subtilis*, with MIC of 125-200 µg/ml and an MBC of 250 µg/ml. Researchers found that AgNPs synthesized using *Ocimum sanctum* showed inhibitory zones ranging from 7-10 mm for *Pseudomonas* and *S. aureus*, with MIC ranging from 125-200 µg/ml and an MBC of 250 µg/ml. In comparison, the *Cl*-AgNPs in the current study demonstrated inhibitory zones of 8 mm for *E. coli* and 6 mm for *S. aureus*, with MIC of 150-200 µg/ml and an MBC of 200 µg/ml. Beyond comparable bactericidal efficacy, *Cl*-AgNPs uniquely exhibited ROS-mediated antibacterial action, confirmed via DCFDA fluorescence imaging. The presence of bioactive compounds such as curcumin, flavonoids, and phenolics in the *Cl* extract likely enhances NP surface reactivity and biological performance, making this synthesis method a more efficient, biologically potent, and environmentally friendly alternative to other plant-based approaches.

The antibacterial efficacy of *Cl*-AgNPs was also compared with that of the *Cl*-rhizome extract. The inhibitory zones for *Cl*-AgNPs against *E. coli* and *S. aureus* were 8 mm and 6 mm, respectively, while the zones for *Cl*-rhizome extract were negligible (no inhibition). This demonstrates a significant enhancement in antimicrobial efficacy

upon NP synthesis, likely due to increased surface area, ROS generation, and improved bioavailability.

Moreover, the ROS assay demonstrated enhanced oxidative stress within *E. coli* cells treated with *Cl*-AgNPs, further contributing to membrane disruption and cell death. This ROS-mediated mechanism, combined with NP-induced structural destabilization, underpins the observed antibacterial efficacy. The observed inhibition zones in the well-diffusion assay also supported this trend, with *Cl*-AgNPs producing larger zones of inhibition against *E. coli* than *S. aureus* at equal concentrations. Overall, these results emphasize that the *Cl*-AgNPs might be useful or effective antimicrobial medications, especially against Gram-negative pathogens. Their dual action, mechanical disruption, and oxidative stress add value to their application in antimicrobial formulations targeting drug-resistant infections.[37,63]

Mechanism/mode of action of AgNPs

The antibacterial activity of *Cl*-AgNPs synthesized using *Cl*-rhizome extract can be attributed to multiple, interrelated mechanisms, as supported by our experimental findings. Notably, the MIC and MBC results demonstrated greater susceptibility of *E. coli* (MIC: 100 µg/ml; MBC: 150 µg/ml) compared to *S. aureus* (MIC: 150 µg/ml; MBC: 200 µg/ml), suggesting that *Cl*-AgNPs are more efficient towards Gram-negative bacteria. This unique response could be because of the differences in the structure of the cell wall; the thinner peptidoglycan layer and outer membrane of the Gram-negative bacteria allow for easier penetration and accumulation of NPs, whereas the thicker peptidoglycan barrier in Gram-positive bacteria offers more resistance.[64]

Further, ROS-mediated oxidative stress was confirmed through the DCFDA assay, treated with *Cl*-AgNPs revealed green fluorescence in *E. coli* cells. This observation shows that *Cl*-AgNPs induce intracellular ROS, leading to membrane rupture, denaturation of proteins, and DNA damage in bacterial cells. Although the ROS analysis was qualitative, it supports the hypothesis that oxidative stress plays an important role in the antibacterial efficacy of *Cl*-AgNPs.[65] The physicochemical properties of the synthesized NPs, particularly their nanoscale size (30-70 nm), spherical morphology, and presence of bioactive surface capping agents, may enhance their interaction with bacterial membranes. These features likely facilitate adhesion, penetration, and subsequent breakdown of the cell membrane, which causes the cell contents to flow out and death of the cell.[66]

Together, the observed antibacterial effects of *Cl*-AgNPs in our study appear to result from a combination of cell membrane interaction, ROS generation, and NP-induced structural damage.[67] These mechanisms are consistent with earlier studies, but are validated in the context of *Cl*-mediated NP synthesis, highlighting the therapeutic potential of plant-based AgNPs in antibacterial applications.[68,69] A detailed representation of this proposed antibacterial mechanism is shown in Figure 9.

CONCLUSION

One of the most efficient and sustainable methods for synthesizing AgNPs involves utilizing plants or plant extracts. These natural sources are abundantly available, environmentally friendly, cost-effective, and rich in diverse biochemical compounds that facilitate NP formation. Among the numerous applications of AgNPs, their antibacterial properties stand out as one of the most extensively researched and utilized. Biofabricated *Cl*-AgNPs have emerged as the key players in the rapidly evolving fields of nanomedicine and nanotherapeutics due to their unique size, shape, and morphological characteristics, making them highly valuable tools for biomedical research and potential clinical applications. However, despite their considerable potential, the detailed antibacterial mechanisms of these NPs are still partially understood.

This study investigates the biological applications of *Cl*-AgNPs, emphasizing their benefits and difficulties encountered in their utilization against bacterial infections. With ongoing advancements in the development of innovative biofabricated NP technology, their role in modern medicine is expected to expand, paving the way for novel therapeutic strategies to improve clinical outcomes. While the present study demonstrates strong *in vitro* antibacterial and antioxidant activities of *Cl*-AgNPs, their *in*

vivo efficacy and biocompatibility remain to be explored. Future studies will focus on evaluating cytotoxicity in mammalian cell lines and assessing *in vivo* bioavailability, immune interaction, and tissue compatibility to determine the adaptive potential of *Cl*-AgNPs for biomedical applications.

Cl-AgNPs exhibit broad application potential across multiple domains, including biomedicine, environmental remediation, agriculture, food preservation, biosensing technologies, and cosmetics. Their synergistic properties, combining the antimicrobial and ROS-scavenging activity of AgNPs with the bioactive benefits of *Cl,* make them an attractive platform for modern nano-based technologies. Future research should emphasize clinical validation and regulatory scaling to translate these applications into real-world use.

Nonetheless, further investigations are necessary to refine AgNP synthesis methods, ensuring precise control over their physicochemical properties while minimizing toxicity and adverse effects. Additionally, a deeper understanding of their mechanisms of action is also crucial for enhancing both biocompatibility and therapeutic efficacy.

A comprehensive grasp of the optimization process, including yield and production efficiency, is essential for achieving precise size control of AgNPs, thereby ensuring their suitability for biomedical and other applications. It is feasible to make AgNPs with well-defined characteristics by carefully adjusting synthesizing parameters, such as precursor concentration, reaction mixture time, temperature of the reaction, pH, and the type of stabilizing agents used. Such optimization is particularly important, as NP size and morphology have a direct impact on biological activities, especially their ability to inhibit or eradicate pathogenic microorganisms responsible for infectious diseases. Moreover, modifications in the proportion and nature of phytoconstituents in the plant extract can also have an immense impact on the surface charge and binding affinity of the forming NPs. These alterations, in turn, affect the particle shape, dispersity, and colloidal stability of AgNPs, underscoring the need for standardized extract preparation to achieve reproducible synthesis outcomes.

Owing to their small size, bioactive curcumin coating, and ROS-generating ability, *Cl*-AgNPs also offer promising potential as nanocarriers for targeted drug delivery. Their surface chemistry supports efficient drug loading, while their interaction with oxidative and inflammatory pathways suggests suitability for responsive delivery systems. Future work should investigate drug encapsulation efficiency and controlled release under physiological conditions, emphasizing their advantages over conventional therapy.

ACKNOWLEDGMENTS

The authors acknowledge the Central Instrumentation Facility (CIF), Lovely Professional University, for providing convenient access to the required instruments. Authors also express their sincere gratitude to Dr. Jiban Jyoti Panda (Scientist-E), Institute of Nano Science and Technology (INST), for granting access to the essential facilities, and to Ms. Swapnil Srivastava (Research Scholar in Dr. Panda's Lab) for her encouragement during the experimentation.

CONFLICT OF INTEREST

The authors declare that there is no conflict of interest.

AUTHORS' CONTRIBUTION

JM conceptualized the study. DSA performed experiments. ANB and DSA conducted analysis. ANB performed data validation. JM and DSA performed data interpretation. DSA wrote the manuscript. ANB and JM performed supervision and reviewed the manuscript. JM revised the manuscript. All authors read and approved the final manuscript for publication.

FUNDING

None.

DATA AVAILABILITY

All datasets generated or analyzed during this study are included in the manuscript.

ETHICS STATEMENT

This article does not contain any studies on human participants or animals performed by any of the authors.

REFERENCES

1. Ansari M, Ahmed S, Abbasi A, et al. Plant-mediated fabrication of silver nanoparticles, process optimization, and impact on the tomato plant. *Sci. Rep.* 2023;13(1):18048. doi: 10.1038/s41598-023-45038-x
2. Tewabe A, Abate A, Tamrie M, Seyfu A, Siraj EA. Targeted Drug Delivery — From Magic Bullet to Nanomedicine: Principles, Challenges, and Future Perspectives. *J Multidiscip*. *Healthc.* 2021;14:1711-1724. doi: 10.2147/JMDH.S313968
3. Baig N, Kammakakam I, Falath W. Nanomaterials: A review of synthesis methods, properties, recent progress, and challenges. *Mater Adv.* 2021;2:1821-1871. doi: 10.1039/D0MA00807A
4. Altammar KA. A review on nanoparticles: characteristics, synthesis, applications, and challenges. *Front Microbiol.* 2023;14:1155622. doi: 10.3389/fmicb.2023.1155622
5. Sharma NK, Vishwakarma J, Rai S, Alomar TS, AlMasoud N, Bhattarai A. Green Route Synthesis and Characterization Techniques of Silver Nanoparticles and Their Biological Adeptness. *ACS Omega*. 2022;7(31):27004-27020. doi: 10.1021/acsomega.2c01400
6. Nie P, Zhao Y, Xu H. Synthesis, applications, toxicity and toxicity mechanisms of silver nanoparticles: A review. *Ecotoxicol Environ Saf.* 2023;253:114636. doi: 10.1016/j.ecoenv.2023.114636
7. Habeeb Rahuman HB, Dhandapani R, Narayanan S, et al. Medicinal plants mediated the green synthesis of silver nanoparticles and their biomedical applications. *IET Nanobiotechnol*. 2022;16(4):115-144. doi: 10.1049/nbt2.12078
8. Alsammarraie FK, Wang W, Zhou P, Mustapha A, Lin M. Green synthesis of silver nanoparticles using turmeric extracts and investigation of their antibacterial activities. *Colloids Surf. B Biointerfaces*. 2018;171:398–405. doi: 10.1016/j.colsurfb.2018.07.059
9. Haugen HJ, Makhtari S, Ahmadi S, Hussain B. The antibacterial and cytotoxic effects of silver nanoparticles coated titanium implants: A narrative review. *Materials*. 2022;15(14):5025. doi: 10.3390/ma15145025
10. Alqahtani MA, Al Othman MR, Mohammed AE. Biofabrication of silver nanoparticles with antibacterial and cytotoxic abilities using lichens. *Sci Rep*. 2020;10(1):16781. doi: 10.1038/s41598-020-73683-z
11. Malik M, Iqbal MA, Malik M, et al. Biosynthesis and characterization of silver nanoparticles from *Annona squamosa* leaf and fruit extracts for size-dependent biomedical applications. *Nanomaterials*. 2022;12(4):616. doi: 10.3390/nano12040616
12. Yin IX, Zhang J, Zhao IS, Mei ML, Li Q, Chu CH. The Antibacterial Mechanism of Silver Nanoparticles and Its Application in Dentistry. *Int J Nanomed*. 2020;15:2555-2562. doi: 10.2147/IJN.S246764
13. Gudikandula K, Charya Maringanti S. Synthesis of silver nanoparticles by chemical and biological methods and their antimicrobial properties. *J. Exp. Nanosci.* 2016;11(9):714-721. doi: 10.1080/17458080.2016.1139196
14. Khan S, Almarhoon ZM, Bakht J, Mabkhot YN, Rauf A, Shad AA. Single Step Acer pentapomicum Mediated Green Synthesis of Silver Nanoparticles and Their Potential Antimicrobial and Antioxidant Activities. *J Nanomater.* 2022;2022(1):3783420. doi: 10.1155/2022/3783420
15. Ahirwar B, Ahirwar D, Jain R, et al. Biofabricated Green Synthesized Hibiscus Silver Nanoparticles Potentiate Antibacterial Activity and Cytotoxicity in Human Lung Cancer Cells. *Appl Biochem Biotechnol.* 2024;196(10):7128-7144. doi: 10.1007/s12010-024-04901-x
16. Altemimi A, Lakhssassi N, Baharlouei A, Watson DG, Lightfoot DA. Phytochemicals: Extraction, isolation, and identification of bioactive compounds from plant extracts. *Plants*. 2017;6(4):42. doi: 10.3390/plants6040042
17. Habibullah G, Viktorova J, Ulbrich P, Ruml T. Effect of the physicochemical changes in the antimicrobial durability of green-synthesized silver nanoparticles during their long-term storage. *RSC Adv.* 2022;12(47):30386-30403. doi: 10.1039/D2RA04667A
18. Rather MA, Deori PJ, Gupta K, et al. Eco-friendly phytofabrication of silver nanoparticles using aqueous extract of *Cuphea carthagenensis* and their antioxidant potential and antibacterial activity against clinically important human pathogens. *Chemosphere*. 2022;300:134497. doi: 10.1016/j.chemosphere.2022.134497
19. El-Saadony MT, Yang T, Korma SA, et al. Impacts of turmeric and its principal bioactive curcumin on human health: Pharmaceutical, medicinal, and food applications: A comprehensive review. *Front. Nutr.* 2023;9:1040259. doi: 10.3389/fnut.2022.1040259
20. Anas M, Falak A, Khan A, et al. Therapeutic potential and agricultural benefits of curcumin: a comprehensive review of health and sustainability applications. *J. Umm Al-Qura Univ. Appl. Sci.* 2024:1-16. doi: 10.1007/s43994-024-00200-7
21. Rodrigues C, Souza VGL, Coelhoso I, Fernando AL. Bio-based sensors for smart food packaging—Current applications and future trends. *Sensors*. 2021;21(6):2148. doi: 10.3390/s21062148
22. Fuloria S, Mehta J, Chandel A, et al. A Comprehensive Review on the Therapeutic Potential of Curcuma longa Linn. in Relation to its Major Active Constituent Curcumin. *Front Pharmacol*. 2022;13:820806. doi: 10.3389/fphar.2022.820806
23. Fuloria S, Mehta J, Chandel A, et al. A Comprehensive Review on the Therapeutic Potential of *Curcuma longa* Linn. in Relation to its Major Active Constituent Curcumin. *Front. Pharmacol.* 2022;13:820806. doi: 10.3389/fphar.2022.820806
24. Sharifi-Rad J, Rayess YE, Rizk AA, et al. Turmeric and Its Major Compound Curcumin on Health: Bioactive Effects and Safety Profiles for Food, Pharmaceutical, Biotechnological and Medicinal Applications. *Front. Pharmacol.* 2020;11:01021. doi: 10.3389/fphar.2020.01021
25. Wulandari A, Sunarti TC, Fahma F, Enomae T. The potential of bioactives as biosensors for the detection of pH. *IOP Conf Ser Earth Environ Sci*. 2020;460(1):012034.

doi: 10.1088/1755-1315/460/1/012034
26. De Oliveira Filho JG, De Almeida MJ, Sousa TL, Dos Santos DC, Egea MB. Bioactive Compounds of Turmeric (*Curcuma longa* L.). In: Murthy, H.N., Paek, K.Y. (eds) *Bioactive Compounds in Underutilized Vegetables and Legumes*. Reference Series in Phytochemistry. Springer, Cham. 2021:297-318. doi: 10.1007/978-3-030-57415-4_37
27. Alam MS, Anwar MJ, Maity MK, Azam F, Jaremko M, Emwas A-H. The Dynamic Role of Curcumin in Mitigating Human Illnesses: Recent Advances in Therapeutic Applications. *Pharmaceuticals*. 2024;17(12):1674. doi: 10.3390/ph17121674
28. Nisa RU, Nisa AU, Tantray AY, et al. Plant phenolics with promising therapeutic applications against skin disorders: A mechanistic review. *J Agric Food Res.* 2024;16:101090. doi: 10.1016/j.jafr.2024.101090
29. Raduly FM, Raditoiu V, Raditoiu A, Purcar V. Curcumin: Modern Applications for a Versatile Additive. *Coatings*. 2021;11(5):519. doi: 10.3390/coatings11050519
30. Al-Otibi FO, Yassin MT, Al-Askar AA, Maniah K. Green biofabrication of silver nanoparticles of potential synergistic activity with antibacterial and antifungal agents against some nosocomial pathogens. *Microorganisms*. 2023;11(4):945. doi: 10.3390/microorganisms11040945
31. Neupane NP, Kushwaha AK, Karn AK, et al. Antibacterial efficacy of bio-fabricated silver nanoparticles of aerial part of *Moringa oleifera* lam: Rapid green synthesis, *In Vitro* and *In Silico* screening. *Biocatal. Agric.Biotechnol.*2022;39:102229. doi: 10.1016/j.bcab.2021.102229
32. Shahzadi S, Fatima S, Ain Q ul, Shafiq Z, Ashraf Janjua MRS. A review on green synthesis of silver nanoparticles (SNPs) using plant extracts: a multifaceted approach in photocatalysis, environmental remediation, and biomedicine. *RSC Adv.* 2025;15(5):3858-3903. doi: 10.1039/D4RA07519F
33. Tawre MS, Shiledar A, Satpute SK, Ahire K, Ghosh S, Pardesi K. Synergistic and antibiofilm potential of *Curcuma aromatica* derived silver nanoparticles in combination with antibiotics against multidrug-resistant pathogens. *Front. Chem.* 2022;10:1029056. doi: 10.3389/fchem.2022.1029056
34. Kordy MG, Abdel-Gabbar M, Soliman HA, et al. Phyto-capped Ag nanoparticles: green synthesis, characterization, and catalytic and antioxidant activities. *Nanomaterials*. 2022;12(3):373. doi: 10.3390/nano12030373
35. Rana N, Banu AN, Kumar B, et al. Phytofabrication, characterization of silver nanoparticles using Hippophae rhamnoides berries extract and their biological activities. *Front. Microbiol.* 2024;15:1399937. doi: 10.3389/fmicb.2024.1399937
36. Ahmed A, Usman M, Ji Z, et al. Nature-inspired biogenic synthesis of silver nanoparticles for antibacterial applications. *Mater Today Chem.* 2023;27:101339. doi: 10.1016/j.mtchem.2022.101339
37. Maghimaa M, Alharbi SA. Green synthesis of silver nanoparticles from *Curcuma longa* L. and coating on the cotton fabrics for antimicrobial applications and wound healing activity. *J Photochem Photobiol B*. 2020;204:111806.doi: 10.1016/j.jphotobiol.2020.111806
38. Parvekar P, Palaskar J, Metgud S, Maria R, Dutta S. The minimum inhibitory concentration (MIC) and minimum bactericidal concentration (MBC) of silver nanoparticles against *Staphylococcus aureus*. *Biomater Investig Dent.* 2020;7(1):105-109. doi: 10.1080/26415275.2020.1796674
39. Sow IS, El Manssouri N, Yang D. Reactive Oxygen Species Production from Hydroxamic Acid and their Iron (III) Complexes against *Staphylococcus aureus* and *Escherichia coli*. *J Clin Intensive Care Med*. 2024;9(1):017–20. doi: 10.29328/journal.jcicm.1001048
40. Bergal A, Matar GH, Andac M. Olive and green tea leaf extracts mediated green synthesis of silver nanoparticles (AgNPs): comparison investigation on characterizations and antibacterial activity. *BioNanoSci*. 2022;12(2):307-321. doi: 10.1007/s12668-022-00958-2
41. Shameli K, Bin Ahmad M, Jaffar Al-Mulla EA, et al. Green biosynthesis of silver nanoparticles using *Callicarpa maingayi* stem bark extraction. *Molecules*. 2012;17(7):8506-8517. doi: 10.3390/molecules17078506
42. Joshi SJ, Geetha SJ, Al-Mamari S, Al-Azkawi A. Green synthesis of silver nanoparticles using pomegranate peel extracts and its application in photocatalytic degradation of methylene blue. *Jundishapur J. Nat. Pharm. Prod.* 2018;13(3):67846. doi: 10.5812/jjnpp.67846
43. Zhou M, LI F, Chen J, Wu Q, Zou Z. Research progress on natural bio-based encapsulation system of curcumin and its stabilization mechanism. *Food Sci. Technol.* 2022;42(11):e78422. doi: 10.1590/fst.78422
44. Van Nong H, Hung LX, Thang PN, et al. Fabrication and vibration characterization of curcumin extracted from turmeric (*Curcuma longa*) rhizomes of northern Vietnam. *SpringerPlus*. 2016;5:1147. doi: 10.1186/s40064-016-2812-2
45. Vanlalveni C, Lallianrawna S, Biswas A, Selvaraj M, Changmai B, Rokhum SL. Green synthesis of silver nanoparticles using plant extracts and their antimicrobial activities: A review of recent literature. *RSC Adv.* 2021;11 (5):2804-2837. doi: 10.1039/D0RA09941D
46. Gong X, Suryamiharja A, Zhou H. pH-Induced Structural Changes of Crystalline Curcumin Enhance Its Encapsulation in Emulsions. *ACS Food Sci Technol.* 2024;4(12):2998-3006.doi: 10.1021/acsfoodscitech.4c00595
47. Philip A, Kumar AR. The performance enhancement of surface plasmon resonance optical sensors using nanomaterials: A review. *Coord Chem Rev.* 2022;458(11):214424. doi: 10.1016/j.ccr.2022.214424
48. Melkamu WW, Bitew LT. Green synthesis of silver nanoparticles using *Hagenia abyssinica* (Bruce) JF Gmel plant leaf extract and their antibacterial and anti-oxidant activities. *Heliyon*. 2021;7(11):e08459. doi: 10.1016/j.heliyon.2021.e08459
49. Kulkarni D, Sherkar R, Shirsathe C, et al. Biofabrication of nanoparticles: sources, synthesis, and

biomedical applications. *Front. Bioeng. Biotechnol.* 2023;11:1159193. doi: 10.3389/fbioe.2023.1159193

50. Alaabedin AAZ, Majeed AMA, Hamza BH. Green synthesis of silver nanoparticles and their effect on the skin determined using IR thermography. *Kuwait J. Sci.* 2024;51(1):100076. doi: 10.1016/j.kjs.2023.07.002
51. Efavi JK, Nyankson E, Kyeremeh K, Manu GP, Asare K, Yeboah N. Monodispersed AgNPs Synthesized from the Nanofactories of *Theobroma cacao* (Cocoa) Leaves and Pod Husk and Their Antimicrobial Activity. *Int. J. Biomater.* 2022;2022:4106558. doi: 10.1155/2022/4106558
52. Ciuca MD, Racovita RC. Curcumin: Overview of extraction methods, health benefits, and encapsulation and delivery using microemulsions and nanoemulsions. *Int. J. Mol. Sci.* 2023;24(10):8874. doi: 10.3390/ijms24108874
53. Alharbi NS, Alsubhi NS, Felimban AI. Green synthesis of silver nanoparticles using medicinal plants: Characterization and application. *J Radiat Res Appl Sci.* 2022;15(3):109-124. doi: 10.1016/j.jrras.2022.06.012
54. Palithya S, Gaddam SA, Kotakadi VS, Penchalaneni J, Challagundla VN. Biosynthesis of silver nanoparticles using leaf extract of *Decaschistia crotonifolia* and its antibacterial, antioxidant, and catalytic applications. *Green Chem Lett Rev.* 2021;14(1):137-152. doi: 10.1080/17518253.2021.1876172
55. Urnukhsaikhan E, Bold B-E, Gunbileg A, Sukhbaatar N, Mishig-Ochir T. Antibacterial activity and characteristics of silver nanoparticles biosynthesized from *Carduus crispus*. *Sci. Rep.* 2021;11(1):21047. doi: 10.1038/s41598-021-00520-2
56. Liaqat N, Jahan N, Khalil-Ur-Rahman, Anwar T, Qureshi H. Green synthesized silver nanoparticles: Optimization, characterization, antimicrobial activity, and cytotoxicity study by hemolysis assay. *Front Chem.* 2022;10:952006. doi: 10.3389/fchem.2022.952006
57. Yadav R, Preet S. Comparative assessment of green and chemically synthesized glutathione-capped silver nanoparticles for antioxidant, mosquito larvicidal, and eco-toxicological activities. *Sci. Rep.* 2023;13(1):8152. doi: 10.1038/s41598-023-35249-7
58. Gupta A, Briffa SM, Swingler S, et al. Synthesis of Silver Nanoparticles Using Curcumin-Cyclodextrins Loaded into Bacterial Cellulose-Based Hydrogels for Wound Dressing Applications. *Biomacromolecules*. 2020;21(5):1802-1811. doi: 10.1021/acs.biomac.9b01724
59. Sharma M, Monika, Thakur P, Saini RV, Kumar R, Torino E. Unveiling antimicrobial and anticancerous behavior of AuNPs and AgNPs moderated by rhizome extracts of *Curcuma longa* from diverse altitudes of Himalaya. *Sci Rep.* 2020;10(1):10934.doi: 10.1038/s41598-020-67673-4
60. Bera D, Pal K, Ruidas B, et al. A mechanistic insight into the bioaccesible herbometallic nanodrug as potential dual therapeutic agent. *Mater Today Commun*. 2020;24:101099. doi: 10.1016/j.mtcomm.2020.101099
61. Karanam G, Arumugam MK. Reactive oxygen species generation and mitochondrial dysfunction for the initiation of apoptotic cell death in human hepatocellular carcinoma HepG2 cells by a cyclic dipeptide Cyclo(-Pro-Tyr). *Mol Biol. Rep*. 2020;47(5):3347-3359. doi: 10.1007/s11033-020-05407-5
62. Huang, MT. Antioxidant and Antitumorigenic Properties of Curcumin. In: Ohigashi, H., Osawa, T., Terao, J., Watanabe, S., Yoshikawa, T. (eds) *Food Factors for Cancer Prevention.* Springer, Tokyo. 1997:249-252. doi: 10.1007/978-4-431-67017-9_50
63. Meikle TG, Dyett BP, Strachan JB, White J, Drummond CJ, Conn CE. Preparation, Characterization, and Antimicrobial Activity of Cubosome Encapsulated Metal Nanocrystals. *ACS Appl Mater Interfaces*. 2020;12(6):6944-6954. doi: 10.1021/acsami.9b21783
64. Dakal TC, Kumar A, Majumdar RS, and Yadav V. Mechanistic basis of antimicrobial actions of silver nanoparticles. *Front. Microbiol*. 2016; 7:1831. doi: 10.3389/fmicb.2016.01831
65. Ali HM, Karam K, Khan T, Wahab S, Ullah S, Sadiq M. Reactive oxygen species induced oxidative damage to DNA, lipids, and proteins of antibiotic-resistant bacteria by plant-based silver nanoparticles. *3 Biotech*. 2023;13(12):414. doi: 10.1007/s13205-023-03835-1
66. Gurunathan S, Han JW, Kwon DN, Kim JH. Enhanced antibacterial and anti-biofilm activities of silver nanoparticles against Gram-negative and Gram-positive bacteria. *Nanoscale Res Lett.* 2014;9(1):373. doi: 10.1186/1556-276X-9-373
67. Dias LD, Blanco KC, Mfouo-Tynga IS, Inada NM, Bagnato VS. Curcumin as a photosensitizer: From molecular structure to recent advances in antimicrobial photodynamic therapy. *J Photochem Photobiol C Photochem Rev.* 2020;45:100384. doi: 10.1016/j.jphotochemrev.2020.100384
68. Ahmad SA, Das SS, Khatoon A, et al. Bactericidal activity of silver nanoparticles: A mechanistic review. *Mater Sci Energy Technol.* 2020;3:756-769. doi: 10.1016/j.mset.2020.09.002
69. Dakal TC, Kumar A, Majumdar RS, Yadav V. Mechanistic basis of antimicrobial actions of silver nanoparticles. *Front Microbiol.* 2016;7:1831. doi: 10.3389/fmicb.2016.01831